Improved forest height estimation by fusion of simulated GEDI Lidar data and TanDEM-X InSAR data

Citation for published version:
Qi, W, Lee, S, Hancock, S, Luthcke, S, Tang, H, Armston, J & Dubayah, R 2019, 'Improved forest height estimation by fusion of simulated GEDI Lidar data and TanDEM-X InSAR data', *Remote Sensing of Environment*, vol. 221, pp. 621-634. https://doi.org/10.1016/j.rse.2018.11.035

Digital Object Identifier (DOI):
10.1016/j.rse.2018.11.035

Improved forest height estimation by fusion of simulated GEDI Lidar data and TanDEM-X InSAR data

Wenlu Qi [a], Seung-Kuk Lee [b], Steven Hancock [a], Scott Luthcke [b], Hao Tang [a], John Armston [a], Ralph Dubayah [a]

[a] Department of Geographical Sciences, University of Maryland, College Park, MD, USA

[b] NASA Goddard Space Flight Center, Greenbelt, MD, USA

ABSTRACT

Interferometric Synthetic Aperture Radar (InSAR) and lidar are increasingly used active remote sensing techniques for forest structure observation. The TanDEM-X (TDX) InSAR mission of German Aerospace Center (DLR) and the upcoming Global Ecosystem Dynamics Investigation (GEDI) of National Aeronautics and Space Administration (NASA) together may provide more accurate estimates of global forest structure and biomass via their synergic use. In this paper, we explored the efficacy of simulated GEDI data in improving height estimates from TDX InSAR data. Our study sites span three major forest types: a temperate forest, a mountainous conifer forest, and a tropical rainforest. The GEDI lidar coverage was simulated for the full nominal two-year mission duration, under both cloud-free and 50%-cloud conditions. We then used these GEDI data to parameterize the Random Volume over Ground (RVoG) model driven by TDX imagery. In particular, we explored the following three strategies for forest structure estimation: 1) TDX data alone; 2) TDX + GEDI-derived digital terrain model (DTM); and 3) TDX + GEDI DTM + GEDI canopy height. We then validated the retrieved forest heights against wall-to-wall airborne lidar measurements. We found relatively large biases at 90 [m] spatial resolution, from 4.2 – 11.9 [m], and root mean square errors (RMSEs), from 7.9 – 12.7 [m] when using TDX data alone under constrained RVoG assumptions of a fixed extinction coefficient (σ) and a zero ground-to-volume amplitude ratio (μ=0). Results improved significantly with the aid of a DTM derived from GEDI data which enabled estimation of spatially-varying σ values (vs. fixed extinction) under a μ=0 assumption, with biases reduced to 1.7 – 4.2 [m] and RMSEs to 4.9 – 8.6 [m] across cloudy and cloud-free cases. The best agreement was achieved in the third strategy by also incorporating information of GEDI-derived canopy height to further enhance the RVoG parameters. The improved model, when still assuming μ = 0, reduced biases to less than or close to one meter and further reduced RMSEs to 4.0 – 6.7 [m]. Finally, we used GEDI data to estimate spatially-varying μ in the RVoG model. We found biases of between -0.7 – 0.9 [m] and RMSEs in the range from 2.6 – 7.1 [m] over the three sites. Our results suggest that use of GEDI data improves height inversion from TDX, providing heights at more accuracy than can be achieved by TDX alone, and enabling wall-to-wall height estimation at much finer spatial resolution than can be achieved by GEDI alone.

Keywords:

Forest height; Lidar; GEDI; ALS; InSAR; TanDEM-X; RVoG

1 Introduction

Forest Above-Ground Biomass (AGB) has been identified as a key parameter for assessing the role of forests in the global carbon cycle and for analyzing ecosystem productivity. However, current quantification of forest AGB worldwide and associated biomass changes remain uncertain (CEOS 2014; Pan et al. 2011). Forest inventory methods have been widely used to estimate AGB at field scales, either through destructive sampling or by measurement of various biomass-related forest structural properties and a subsequent employment of allometric equations. However, these methods are often labor-intensive and time-consuming, and do not yield continuous AGB maps over the landscape (Clark and Kellner 2012; Duncanson et al. 2015a; Duncanson et al. 2015b; Keller et al. 2001). Therefore, there is an interest to capitalize on field-scale biomass and remotely measured forest parameters (particularly height) to provide more cost-effective AGB mappings at large areas (Goetz and Dubayah 2011; Huang et al. 2012).

Lidar and Interferometric Synthetic Aperture Radar (InSAR) remote sensing techniques are playing increasingly important roles in estimating important forest structural attributes (Goetz and Dubayah 2011; Hajnsek et al. 2009; Hall et al. 2011). These attributes have been related to field-based biomass estimates for mapping forest AGB over the landscape using both parametric (Nelson et al. 2017; Solberg et al. 2013) and non-parametric modeling techniques (Blackard et al. 2008; Kellndorfer et al. 2012). However, taken individually, each technique has particular limitations and difficulties to deliver large-area forest structure dataset for reducing the uncertainty of forest AGB quantification (Goetz and Dubayah 2011; Hall et al. 2011). Lidar-based biomass estimates are mainly restricted to local regions where airborne lidar campaigns were conducted (Drake et al. 2003; Huang et al. 2012; Swatantran et al. 2011). Data from the sole spaceborne Earth observation lidar instrument, Geoscience Laser Altimeter System (GLAS) onboard Ice, Cloud, and land Elevation Satellite (ICESat), have been used to produce consistent forest structure AGB maps at the continental or global scales by integrating with other spaceborne remote sensing data, such as radar and multispectral observations. However, unless aggregated to coarse resolutions (often larger than a few kilometers) these estimates were often associated with large uncertainties, primarily due to the low sensitivity of the used ancillary data to the full range of forest vertical structure and biomass, and the low sampling density of GLAS, particularly over mid-latitude and tropical forests (Baccini et al. 2012; Hu et al. 2016; Nelson et al. 2017; Saatchi et al. 2011).

InSAR has been widely used to generate wall-to-wall forest structure and biomass maps (Lei and Siqueira 2015; Schlund et al. 2015; Soja et al. 2014). However, accuracies of InSAR products are often reduced by temporal decorrelation which occurs when the SAR images forming the interferometric coherence are acquired at different times. This temporal decorrelation limits the accuracy of repeat-pass interferometry (Lavalle and Hensley 2015; Lee et al. 2013; Papathanassiou and Cloude 2003). To address this problem, the German Aerospace Center (DLR) launched the first dual-satellite (bistatic) SAR spaceborne mission – TanDEM-X (TDX). There is no temporal decorrelation using TDX because the data from each satellite are obtained at the same time, allowing more accurate estimation of forest height and biomass (Askne et al. 2013; Kugler et al. 2014; Persson et al. 2017; Treuhaft et al. 2015). A simple forest scattering model, the Random Volume over Ground (RVoG) model, has been widely used to produce forest height maps from TDX coherence under a variety of terrain conditions and forest types. However, because TDX images are generally acquired at a single polarization, determination of forest height using the RVoG model must assume known canopy extinction and topographic parameters (Hajnsek et al. 2009; Kugler et al. 2014; Qi and Dubayah 2016).

The aforementioned issues of lidar and InSAR potentially may be addressed by combining their complementary observations, where lidar data are used to constrain the forest scattering model and to validate InSAR height inversion while InSAR images are exploited to extend lidar observations (Bergen et al. 2009; Goetz and Dubayah 2011; Hall et al. 2011; Qi and Dubayah 2016; Sun et al. 2011). For example, previous studies have used airborne lidar elevation data to provide the needed external DTM to estimate forest height from TDX single-polarization (single-pol) coherence

(Cloude et al. 2013; Kugler et al. 2014; Schlund et al. 2015; Soja and Ulander 2013; Solberg et al. 2013). Accurate airborne lidar observations of forest vertical structure have also been used to enhance parameterization of the forest scattering models for improved forest height estimation (Brolly et al. 2016). The elevation data derived from the first spaceborne InSAR mission – Shuttle Radar Topography Mission (SRTM) – has been calibrated and validated with local height measurements from GLAS to produce continuous canopy height and AGB maps over Mangrove forests (Fatoyinbo and Simard 2013). These studies have demonstrated the potential advantages in combining lidar and InSAR to map forest structure at better accuracy and coverage.

An unprecedented opportunity of global forest structure and biomass mapping from lidar/InSAR fusion has emerged with the upcoming launch of the Global Ecosystem Dynamics Investigation (GEDI) mission (Qi and Dubayah 2016). GEDI is a full-waveform lidar system to be deployed on the International Space Station (ISS) by NASA in 2018 (Stysley et al. 2015). During its nominal two-year mission, GEDI will provide about 15 billion ground elevation and forest vertical structure measurements at a footprint size of ~25 m in diameter. Aided by these GEDI observations, TDX data can potentially provide wall-to-wall forest height maps, which in turn can be used to extend GEDI observations for forest structure and biomass estimation at finer resolution, accuracy and coverage (Qi and Dubayah 2016). However, the effects of using different elements of forest vertical structure observed by GEDI on TDX height inversion are still unclear and largely unexplored. Also, the performance of GEDI/TDX fusion needs to be investigated for different forest structural types and environmental conditions.

The goal of this paper is to develop lidar/InSAR fusion methods for improved TDX height estimates using GEDI observations. GEDI data are simulated using airborne laser scanning (ALS) data and combined with single-pol TDX InSAR data. Our test sites include three contrasting forest types: Hubbard Brook Experimental Forest (HBEF), a temperate mixed broadleaf deciduous and conifer forest; Teakettle Experimental Forest (TEF), a mountainous conifer forest; and La Selva Biological Station (LSBS), a tropical broadleaf rainforest. Specifically we perform three sets of analyses to explore the impact on height derivations using fusion. First, we establish a baseline accuracy for our study sties by using only TDX data and simple assumptions of RVoG parameters. Next, we utilize an external DTM derived from simulated GEDI data in the RVoG model. Lastly, we investigate the impact of using both a simulated GEDI DTM and GEDI-derived canopy heights within the RVoG model. In each case, we also examine the impact of clouds and phenology on the fusion results by comparison of GEDI tracks under cloud-free vs. 50%-cloud conditions, and comparison of leaf-on vs. leaf-off TDX acquisitions. Results from this study should help inform potential approaches towards improved mapping of forest height and biomass using lidar and InSAR remote sensing.

2 Test Sites and Data

2.1 Test sites

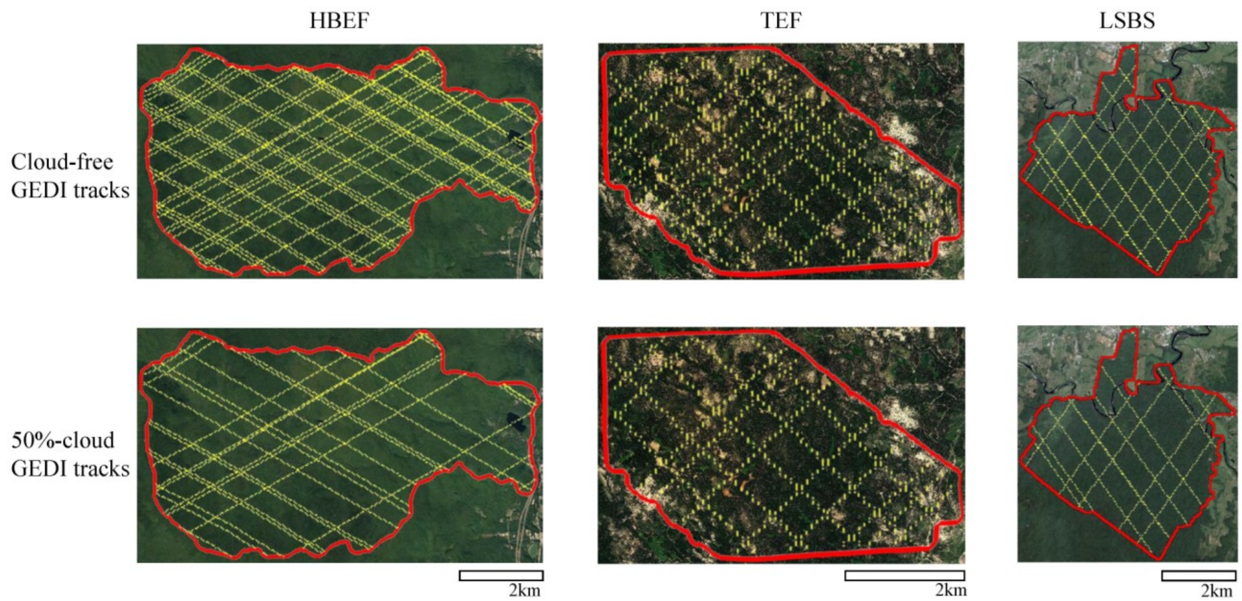

Fig. 1 Simulated two-year GEDI tracks over HBEF, TEF and LSBS test sites respectively based on cloud-free and 50%-cloud cover conditions.

Three sites were chosen, representing a range of forest characteristics (Fig. 1). Hubbard Brook Experimental Forest (HBEF) (43°56′12″N, 71°45′01″W) is a closed-canopy broadleaf-dominated forest located in the White Mountain National Forest, New Hampshire, USA, and is typical of temperate forest conditions. Covering an area of 3,100 ha the topography of the site is rugged, with steep slopes occurring within a bowl-shaped watershed. Elevations range from about 150 m to 1000 m. It is a managed forest consisting of mostly deciduous northern hardwoods and a small percentage (10–20%) of spruce-fir. Measured forest heights mainly range from ~2 to ~42 m, with a mean of ~24 m and a standard deviation of ~5 m. HBEF has a moderate amount of above ground biomass, with a mean of 216 Mg/ha in 2001 (Qi and Dubayah 2016; Schwarz et al. 2001; Siccama et al. 2007; Whitehurst et al. 2013).

Teakettle Experimental Forest (TEF) (36°57′60″N, 119°01′0″W) is a conifer-dominated forest located along the western slopes of Sierra Nevada Mountain Range, USA. The study site is a mountainous region covering an area of around 1,300 ha, with elevations ranging from about 1,800 m to 2,500 m elevation. It is an old-growth forest with mature and complex structure. Tree heights mainly range from ~3 m to ~68 m, with a mean height of ~39 m and a standard deviation of ~11 m. Major tree types include White fir (*Abies concolor*), Ponderosa pine (*Pinus ponderosa*), Red fir (*Abies magnifica*) and California black oak (*Quercus kellogi*) (Pierce et al. 2002). The averaged aboveground biomass is about 200 Mg/ha with individual tree values up to 20 Mg per tree (Duncanson et al. 2015a; Smith et al. 2005; Swatantran et al. 2011).

La Selva Biological Station (LSBS) (10°25′44″N, 84°00′29″W) is a low-land (elevation <150 m) tropical rain forest in northeastern Costa Rica. The site is a protected region covering about 1,600 ha, and contains a mixture of old-growth, secondary and selectively logged forests as well as agroforestry plantations, developed areas, and abandoned pastures. Tree height ranges from ~3 to ~59 m, with a mean of ~28 m and a standard deviation of ~11 m. Estimate of aboveground biomass spans from 0 to 279 Mg/ha, and averaged biomass of old-growth forest, which is the major components of total LSBS biomass, is around 169 Mg/ha (Clark et al. 2011). Detailed site characteristics can be found in (Clark et al. 2008; Dubayah et al. 2010; Tang et al. 2014; Tang et al. 2012).

2.2 Datasets

2.2.1 Airborne lidar data

Small-footprint discrete return lidar data were collected over HBEF in September 2009 when trees were in leaf-on condition. An Optech ALTM 3100 instrument collected data with an average point density of 4.0 shots per square meter, and up to four returns for each laser shot. In September 2008, the Optech Gemini instrument flew over TEF to acquire lidar data at an averaged point density of 14.7 shots per square meter, with up to four returns per laser shot. At LSBS, the lidar data were collected in September and October of 2009. The Optech ALTM 3100EA instrument was used for this site, and achieved an averaged point density of 3.0 per square meter and up to four returns per laser shot. All these lidar surveys were carried out in clear sky conditions. There were no clouds, precipitation, atmospheric haze or blowing snow to affect the accuracy of the lidar measurements. These data were processed to simulate GEDI full-waveform data following the method of Blair and Hofton (1999) with measurement noise added following Hancock et al. (2011), summarized briefly in Section 2.2.2. It is demonstrated in a separate simulator validation paper that the GEDI simulator accurately creates full-waveform, large-footprint lidar signals from data from all ALS instruments and beam densities in these investigations (Hancock et al. 2019).

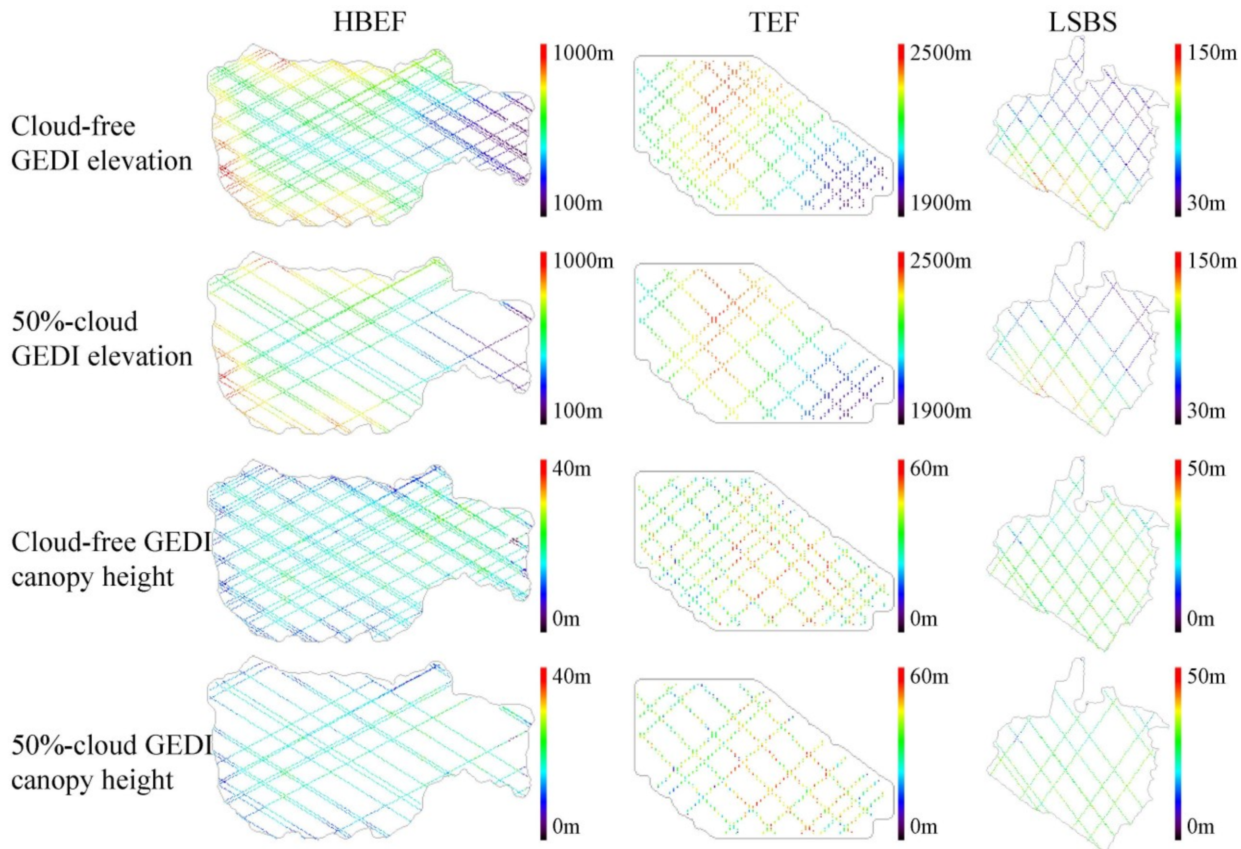

Fig. 2 Simulated GEDI observations of elevation and canopy height over nominal two-year period based on cloud-free and 50%-cloud cover conditions.

2.2.2 Simulated GEDI observations from ALS data

Our GEDI simulation in this study is based on an earlier system configuration. In this configuration, GEDI was comprised of three identical lasers (Coyle et al. 2015; Stysley et al. 2015), two of which were split into four beams (what we call "coverage beams"). The power of the coverage beam after splitting was about half that of the strong beam. These five beams were dithered across-track on every other line to produce 10 parallel ground tracks with approximately 600 m spacing across track and 60 m spacing along track. The GEDI across-track ground swath width (the distance from beams 1 to 10) was therefore approximately 5.4 km. The inclination of tracks relative to north, determined by the inclination of the ISS orbit (Qi and Dubayah 2016), was, and still is, latitude-dependent and thus different for each site (see Fig. 1). After simulating the likely number of times the 10-beam pattern of GEDI would cross each site after the full two-year period, we obtained the track patterns for leaf-on orbits under cloud-free condition as shown in the upper row of Fig. 1.

The finalized GEDI lidar system to be deployed on ISS has a different configuration. Only one of the three lasers is split into two coverage beams and the other two lasers are not split. This new configuration produces a total of four beams (two coverage and two full power beams) and thus eight parallel ground tracks after beam dithering. The spacings of footprints across track and along track are not changed, being about 600 m and 60 m respectively. The ground swath width is thus approximately 4.2 km. This eight-beam pattern of GEDI generally gives about 20% less GEDI footprints compared to those provided by a 10-beam pattern GEDI within our simulations here, and the difference should have a small impact on our results, as discussed later in Section 5.

Since future local cloud conditions for each GEDI orbital pass are unknown, an estimate of ~50% for the mean global cloud cover (Downs and Day 2005) was applied to obtain the track patterns under cloudy condition for all sites (see lower row in Fig. 1). Specifically, the impact of data losses due to cloud cover was simulated by removing complete GEDI tracks. For each track, a random number (0-1) was selected and if that number was greater than the cloud over (0.5), it was used. If it was less, all GEDI footprints in that track were rejected. This assumes that the cloud length scale was large enough to remove a complete track, but not so large that adjacent tracks were affected. Both track patterns under cloud-free and 50%-cloud conditions were then used as templates for the extraction of ALS-derived waveforms to simulate GEDI observations (see Fig. 2).

In the simulation process, GEDI is modelled as a Gaussian shaped laser footprint with a width (1 sigma) of 5.5 m (an effective footprint size of 22 m) a near Gaussian outgoing laser pulse shape of length (full width half maximum) 15.6 ns and a range resolution of 15 cm. The expected signal to noise ratio has been estimated for mean atmospheric transmission and surface reflectance and a 3 db loss of link margin added to make predictions more conservative. To simulate GEDI signals, discrete return ALS points are taken to be representative of the vertical distribution of surfaces. All ALS points within 17.4 m horizontally of the footprint center were included (corresponding to an intensity of 0.06 % of the maximum). The contribution of each was weighted by the GEDI footprint intensity at that point, convolved along the vertical axis by the outgoing laser pulse shape and added up into an array binned to 15 cm resolution. White Gaussian noise was added to give the expected signal-to-noise ratio (Davidson and Sun 1988; Hancock et al. 2011).

A "truth" ground elevation was identified from the high-resolution ALS data (Isenberg 2011) and canopy height was calculated relative to that ground surface as the 98^{th} percentile (RH98) (Drake et al. 2002).

The simulated GEDI waveforms were processed to extract waveform metrics. Denoising was achieved by smoothing the waveform by a Gaussian of FWHM 11ns (75% of GEDI system pulse) (Hofton et al. 2000). The mean and standard deviation of the noise was calculated from the values of the first 10 m of each waveform. The mean noise was subtracted and a threshold was set equal to 3.5 times the standard deviation. All signal not greater than the threshold for at least three consecutive waveform bins was set to zero. The ground was identified by Gaussian fitting to the denoised waveforms (Hofton et al. 2000) and relative height (RH) metrics calculated. The GEDI estimate of height was taken as the 98^{th} percentile (RH98) (Drake et al. 2002).

2.2.3 TDX data

The simulated GEDI data were based on ALS data acquired pre-TDX-launch. We therefore used TDX acquisitions closest in time, to minimize temporal discrepancies. Specifically, TDX acquisitions in 2011 were used for TEF and LSBS test sites; for HBEF, both 2011 (leaf-on) and 2012 (leaf-off) acquisitions were used (Table 1). Selection of TDX data within the desired temporal windows was further refined based on their Height of Ambiguity (*HoA*) values. *HoA* can be calculated as $2\pi/\kappa_z$ (see Section 3.1 for the definition of κ_z and its use in RVoG model) and defines the maximum height retrieval allowed by a specific acquisition geometry (Kugler et al. 2015). In terms of polarization state, we only explored *HH* data because of its availability at the global scale (Krieger et al. 2007; Kugler et al. 2014). All data were acquired in bistatic mode, where one satellite was transmitting and both satellites were simultaneously receiving the returned signal, and thus had no temporal decorrelation effect (Abdullahi et al. 2016; Kugler et al. 2014; Lee and Fatoyinbo 2015).

The time difference between the ALS and TDX acquisitions was 2–3 years for HBEF, 3 years for TEF and 2 years for LSBS. The magnitude of forest change was minor over most undisturbed places within these time intervals (Dubayah et al. 2010; Smith et al. 2005; Van Doorn et al. 2011). All areas disturbed between the acquisition dates of ALS and TDX data were removed using ancillary disturbance product from Landsat images (Huang et al. 2010). No precipitation was observed on the dates of the TDX acquisitions for leaf-on HBEF, TEF and LSBS. However, a high precipitation rate was observed near the acquisition date for leaf-off HBEF (0.20 inches on that day and 0.82 inches on the day before) (NOAA), leading to a different forest water content compared to that observed for the lidar acquisition (Kugler et al., 2014), discussed later in Section 4.

Table 1. Summary of TDX acquisitions over the study areas.

Study area	HBEF (temperate mixed forest)		TEF (mountainous conifer forest)	LSBS (tropical broadleaf forest)
Acq. Date	2011/10/21 (Leaf-on)	2012/01/28 (Leaf-off)	2011/12/10	2011/12/05
Eff. Bsl. (m)	121.42	85.37	103.59	89.43
HoA (m)	-47.43	-68.12	-64.47	67.79
Rg. Res. (m)	2.99	2.99	2.71	1.93
Az. Res. (m)	3.30	3.30	3.30	6.60
Pol.	HH	HH	HH	HH, VV
Inc. Ang. (°)	36.2	36.1	40.7	37.7

*Acq. Date – Acquisition Date (Year/Month/Day); Eff. Bsl. – Effective Baseline; HoA – Height of ambiguity; Rg. Res. – Range Resolution; Az. Res. – Azimuth Resolution; Pol. – Polarization; Inc. Ang. – Incident Angle.

3 Single-polarization RVoG inversion and combination with GEDI data

3.1 RVoG model and height inversion from single-pol InSAR data

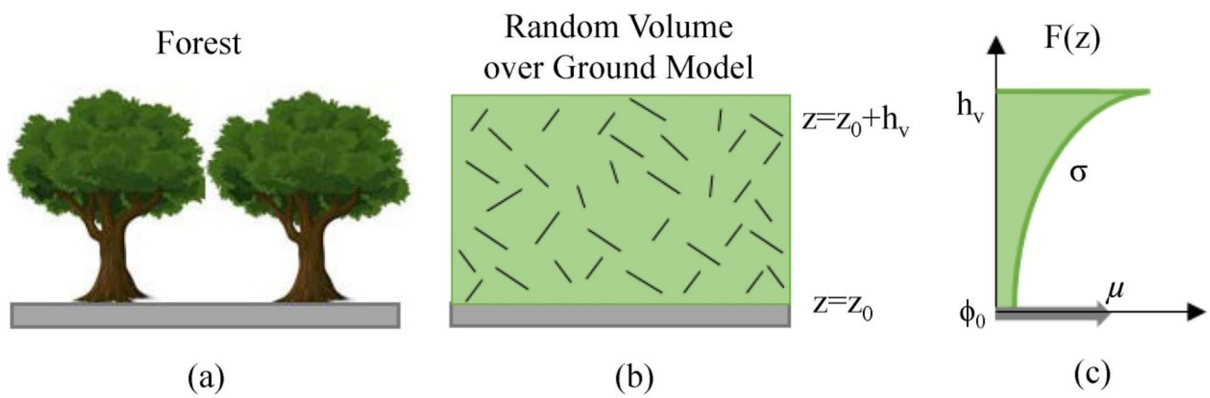

Fig. 3 The basis of the RVOG model. Forest structure in (a) is modeled using the two-layer scattering model in (b) with ground elevation z_0 and volume height (h_V). Scatterers are randomly distributed and oriented inside the forest volume (Cloude and Papathanassiou 2003). *F(z)*, radar reflectivity of forest scatterers at different height z, decays as a function of extinction coefficient (σ) as shown in (c). The term φ_0 denotes the ground phase ($e^{i\varphi_0} = e^{i\kappa_z z_0}$) and μ is the ground-to-volume amplitude ratio (Cloude and Papathanassiou 2003).

Random Volume over Ground (RVoG) model is a widely used two-layer scattering model (see Fig. 3) that enables the inversion of physical forest parameters from InSAR coherences. Based on the RVoG model, the complex interferometric coherence $\tilde{\gamma}$ at a polarization ($\vec{\omega}$), after compensating system and geometry induced decorrelation effects (Kugler et al. 2015), can be simply represented by equation (1),

$$\tilde{\gamma} \qquad \frac{\qquad}{1+\mu(\vec{\omega})} \tag{1}$$

where φ_0 is the phase corresponding to the ground elevation z_0; and $\mu(\vec{\omega})$ denotes the (polarization-dependent) ratio of powers echoed from ground and forest volume (Hajnsek et al. 2009; Kugler et al. 2014; Papathanassiou and Cloude 2001) (Fig. 3). Since this study only works with *HH* TDX data ($\vec{\omega} = HH$), $\tilde{\gamma}$ will be written as $\tilde{\gamma}$ and $\mu(\vec{\omega})$ as μ hereafter. $\tilde{\gamma}$ represents volume coherence and can be described by a Fourier relationship of the vertical profile of the radar reflectivity *F(z)* and the volume height h_V,

$$\tilde{\gamma} \qquad \frac{\int^{h_V} \mathrm{F(z')}\, \mathrm{e}^{i\kappa_z z'}\, dz'}{\int_0^{h_V} \mathrm{F(z')}\, dz'} \tag{2}$$

where κ_z is the effective vertical wavenumber. Therefore, when the ground-to-volume amplitude ratio (μ) was zero, the correlation coefficient $|\tilde{\gamma} \quad \tilde{\gamma}|$. The estimation of h_V requires the parameterization of *F(z)*. A widely and successfully employed approach is to assume that the distribution of scatterers decreases exponentially from the volume top downward, i.e., $F(\mathrm{z}) = e^{\frac{2\sigma}{\cos\theta} z}$ where θ describes the incidence angle and σ, the mean extinction coefficient, represents the attenuation rate of the wave within the volume (see Fig. 3) (Cloude and Papathanassiou 2003; Papathanassiou and Cloude 2001).

Single-pol InSAR inversion is an underdetermined problem, meaning that the number of observables from the interferometric coherence is smaller than the number of the unknown parameters. Previous studies solved this problem with two constraints: 1) using an external digital terrain model (DTM) to estimate ground phase (φ_0) or using a fixed mean extinction coefficient (σ) for the entire study site; and 2) assuming a zero ground-to-volume amplitude ratio (μ=0) at the polarization state of the acquisition. However, external DTMs are often unavailable over large areas, and the accuracy of height inversion may be compromised when a fixed σ (as opposed to one that varies spatially) is used (Hajnsek et al. 2009; Kugler et al. 2014). Also, ground scattering may be present (i.e. $\mu \neq 0$) in areas with low forest density or low vegetation water content (Kugler et al. 2014). To overcome these issues, we assess the efficacy of using GEDI-derived DTM and canopy heights to provide the needed prerequisite information for TDX single-pol inversion.

3.2 *Combining RVoG single-pol InSAR inversion with GEDI data*

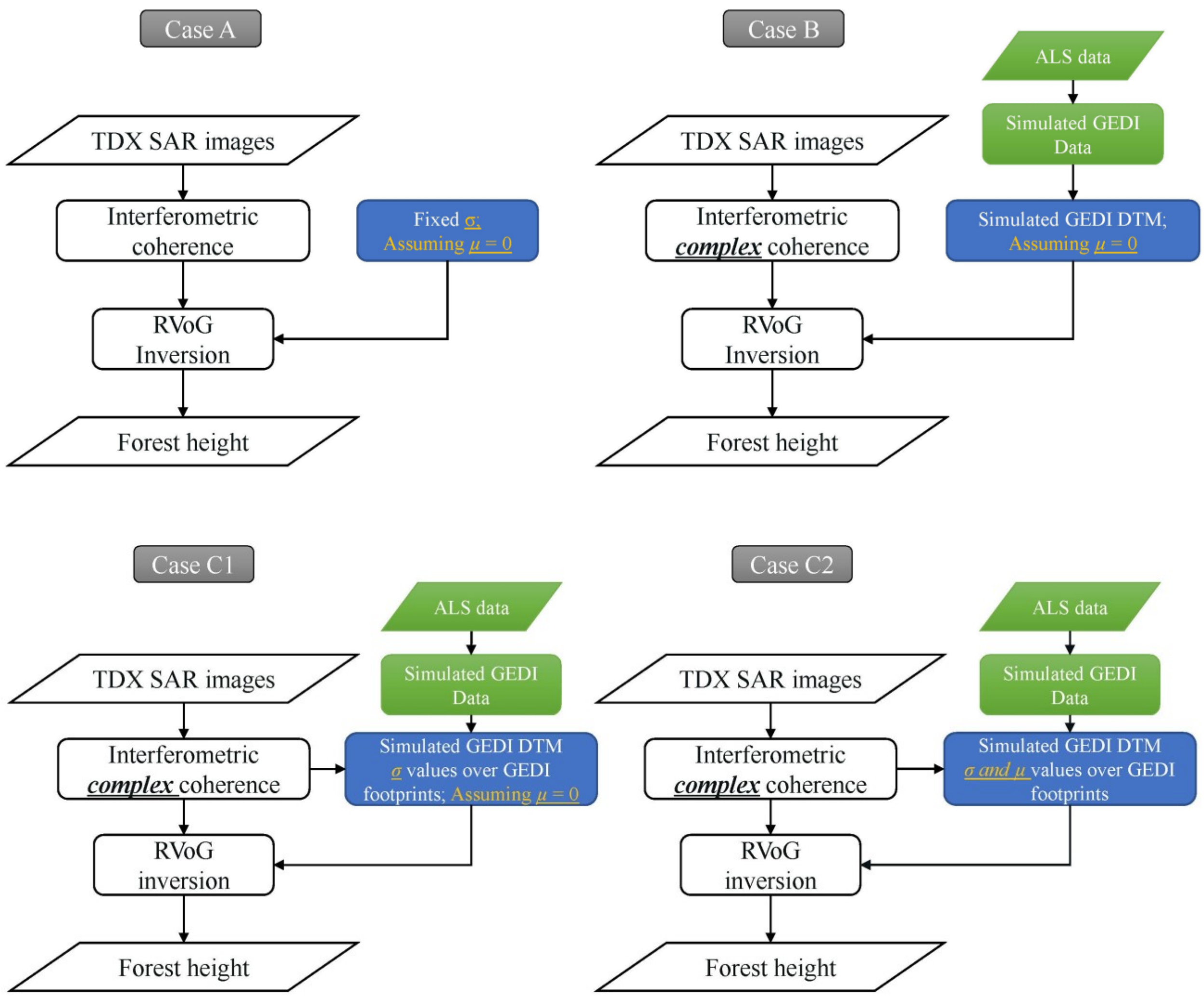

Fig. 4 Main procedures for the four different fusion approaches – cases A, B, C1 and C2.

Table 2. RVoG model parameterization for different cases performed in this study.

Cases	**Used TDX observables**	**Added Inputs for RVoG**	**RVoG parameters**
A Only TDX (Baseline)	Magnitude of coherence	Assumptions for σ and μ	$\sigma = constant$; $\mu = 0$
B Using GEDI DTM	Complex coherence	Ground phase φ_0 from GEDI DTM; Assumption for μ	σ map that is purely data-driven; $\mu = 0$

C1 & C2 Using GEDI height and DTM	Complex coherence	C1) Ground phase φ_0 from GEDI DTM; Forest height over GEDI footprints for estimating σ; Assumption for μ	σ map interpolated from σ values along GEDI tracks; μ = 0
		C2) Ground phase φ_0 from GEDI DTM; Forest height over GEDI footprints for estimating σ and μ	σ and μ maps interpolated from σ and μ values along GEDI tracks

We perform a set of three analyses (Fig. 4) where DTM and tree height variables derived from simulated GEDI Lidar data were added progressively as inputs to improve the parameterization of single-pol RVoG inversion, enabling an examination of the respective performance gain on height estimation.

Case A – Only TDX. This case served as a baseline to assess what improvements in canopy height accuracy, if any, would be achieved from the addition of data derived from GEDI. Here, forest height was derived solely from the magnitude of TDX interferometric coherence $|\tilde{\gamma}|$ (i.e. interferometric correlation coefficient) by using a constant value of extinction coefficient (σ) and a zero ground-to-volume amplitude ratio (μ=0) assumption (see Table 2 case A). A key step of this method is to determine an appropriate σ value that in general represents forest density and dielectric constant for the entire study site. For a particular acquisition with *HoA* larger than forest height, a σ value higher than optimum often leads to an overestimation of h_V whereas a σ value lower than optimum may result in an underestimation of h_V (see Fig. 5) (Caicoya et al. 2012; Hajnsek et al. 2009). The presence of ground scattering that violates the μ=0 assumption may also lead to increased errors in tree height estimation (Kugler et al. 2014). Previous studies found a variation of 0.3 dB/m – 1 dB/m for σ values in temperate leaf-on broadleaf forest (Kugler et al. 2010), 0 – 0.4 dB/m in conifer forest (Caicoya et al. 2012) and 0.1 dB – 0.9 dB/m in tropical broadleaf forest (Hajnsek et al. 2009). Forest heights had been retrieved using a constant σ value of 0.3 dB/m for a tropical forest and a leaf-on temperate forest (Hajnsek et al. 2009; Kugler et al. 2010), and a value of 0.2 dB/m for a conifer forest (Caicoya et al. 2012). In this study, we applied similar σ values of 0.3 dB/m for leaf-on HBEF and LSBS, and 0.2 dB/m for TEF. The relatively smaller extinction of 0.2 dB/m was applied for leaf-off HBEF as better penetration capability of TDX was usually observed for leaf-off deciduous forest due to the relatively lower canopy cover and forest density (Abdullahi et al. 2016; Olesk et al. 2015).

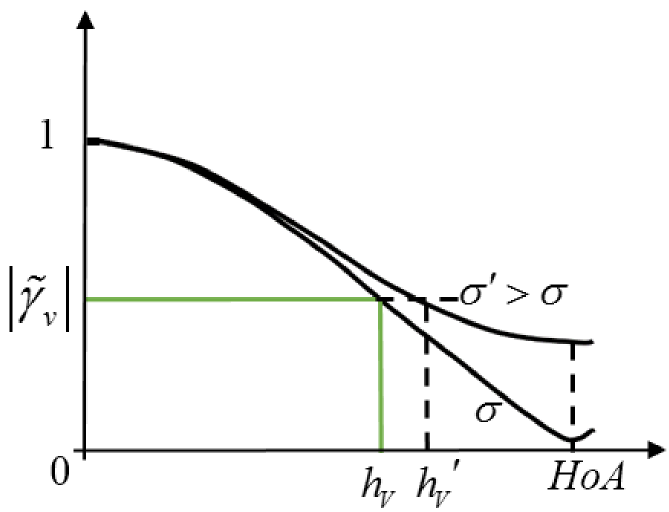

Fig. 5 An increase of h_V up to HoA corresponds to the decrease of $|\tilde{\gamma}_v|$ for a fixed σ. For the same $|\tilde{\gamma}_v|$ value, a higher σ' value derived a larger forest height h_V'.

Case B – Using a simulated GEDI DTM. This case was designed to examine the impact of adding a GEDI-derived DTM on the TDX RVoG inversion. The DTM was created at 30 m resolution using simulated GEDI elevation data and a widely used spherical semivariogram model for the kriging-interpolation method to characterize the spatial autocorrelation of geolocated measurements (Goovaerts 2000; Maselli and Chiesi 2006). Ground phase (φ_0) was estimated from this DTM and subsequently used to derive forest scattering phase (φ); φ equals TDX interferogram ($\varphi_{\_interf}$) subtracted by flat-earth-phase ($\varphi_{\_flat}$) and ground phase φ_0; both $\varphi_{\_interf}$ and $\varphi_{\_flat}$ can be calculated from TDX acquisitions. The scattering phase (φ), combined with the interferometric correlation coefficient ($|\tilde{\gamma}|$), allowed the establishment of a balanced single-pol RVoG inversion after using the μ=0 assumption to derive h_V and σ (see Table 2 case B). Compared to the fixed σ value employed in case A, data-driven σ values may reflect better the variation of forest environment, such as volume density and vegetation water content, and thus enhance the h_V inversion. However, because the accuracy of scattering phase (φ) estimation is sensitive to the accuracy of the GEDI-derived DTM that derived φ_0 (Qi and Dubayah 2016), efficacy of this method is impacted by the available lidar shot density and the local topography variation, i.e. if the DTM is created from sparse data and the topography has large variation at local scales, the kriged DTM may not capture this variation accurately.

Case C1 and C2 – Using a simulated GEDI DTM and GEDI canopy heights. In these two cases, we assessed the effect of using both DTM and canopy height from simulated GEDI data on RVoG height inversion. The auxiliary information from lidar enabled the determination of two RVoG parameters over GEDI tracks (σ and μ), to constrain the inversion. To quantify the performance gain, we designed cases C1 and C2 to parameterize these variables progressively with the added lidar inputs. First, for case C1, we calculated only σ values (kriging was then used to estimate σ for the entire study area), assuming μ=0 as in previous cases, and tested the improvement of h_V estimation (see Table 2 case C1). By constraining σ with the additional input of simulated GEDI canopy height, case C1 was expected to be less sensitive to errors of DTM estimation than case B. Second, to further evaluate the effect of using GEDI-based RVoG parameterization, we calculated both σ and μ values and applied their interpolated maps (based on kriging) to derive h_V (see Table 2 case C2). Over areas where ground scattering is present, we hypothesize that case C2 can reflect better forest structure variation and thus should outperform case C1, which assumed no scattering from ground (i.e. μ=0). For all cases, the derived forest height maps were resampled at 30 m resolution and subsequently averaged to 90 m (using a 3 × 3 window) to compare against reference lidar canopy heights. Note that for cases B, C1 and C2, results along the simulated GEDI tracks were excluded in the averaging and comparison process, considering that the simulated GEDI elevation and/or canopy height data were used to constrain the RVoG model parameterization.

4 Results

4.1 Case A – Only TDX

Following the method described in Section 3.2 (Case A), we derived forest heights directly from TDX correlation coefficient ($|\tilde{\gamma}|$) using fixed σ values of 0.3 dB/m (for leaf-off, 0.2 dB/m was used for leaf-on condition), 0.2 dB/m, and 0.3 dB/m respectively for HBEF, TEF, and LSBS (Fig. 6). As mentioned earlier, for a particular acquisition with *HoA* larger than forest height, the use of a σ value that is too high may result in an overestimation of h_V, and vice versa. Biases of 6.4 m (leaf-on)/11.9 m (leaf-off), 4.2 m and 4.9 m were respectively found for HBEF, TEF and LSBS. These results indicated that optimum σ values may be smaller than those were used here. The particularly large bias at HBEF during leaf-off season may also be related to the violation of the μ=0 assumption as there are areas of low canopy cover that could lead to ground scattering, and a possibly high level of forest water content due to the high precipitation rate near the acquisition date.

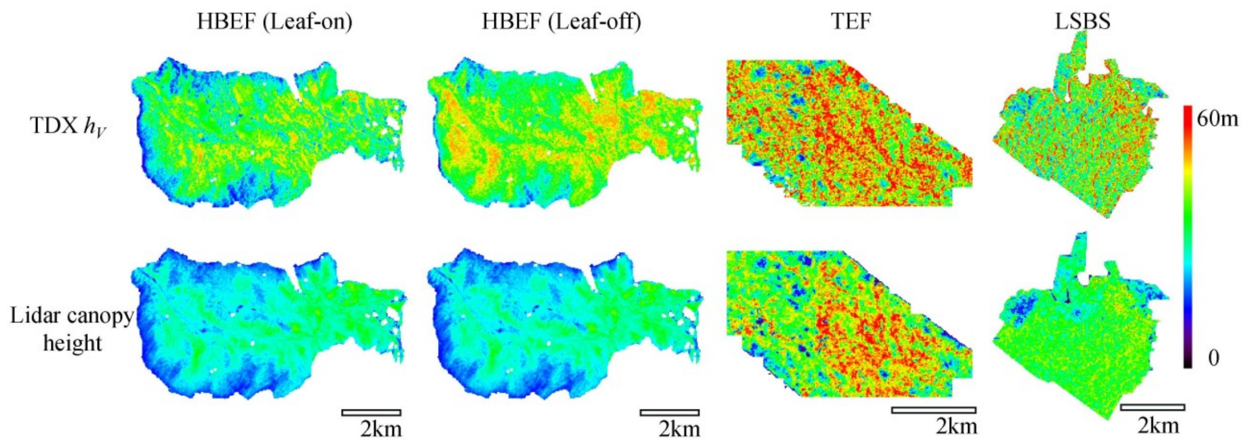

(a)

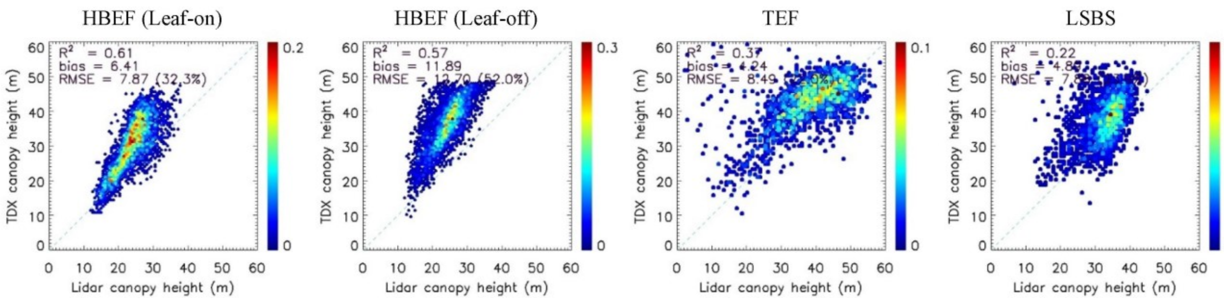

(b)

Fig. 6 (Case A) (a) Forest heights derived using fixed extinction (σ) values of 0.3 dB/m (for leaf-off, 0.2 dB/m was used for leaf-on condition), 0.2 dB/m, and 0.3 dB/m respectively for HBEF, TEF, and LSBS. (b) Comparisons of the derived heights and reference lidar heights at 90 m resolution.

The coefficient of determination observed between the derived heights and reference heights at HBEF was good (r^2 = 0.61 for leaf-on and 0.57 for leaf-off conditions), indicating an overall homogeneous forest structure (because only one σ was given) and good explanatory power of TDX $|\tilde{\gamma}_V|$ at this site. In contrast, lower coefficient of determination were found at TEF (r^2=0.37) and LSBS (r^2=0.22), probably resulting from the lower explanatory power of the used TDX coherences, given that TDX signal is expected to have less penetration capability over areas with taller trees and higher forest density. In addition, these sites have a somewhat heterogeneous forest structure, and therefore an expectation that σ may have a larger spatial variation and thus is less suitable for using the fixed value assumption.

4.2 Case B – Using simulated GEDI DTM

We estimated a scattering phase (φ) map for each site using the external DTM derived from simulated GEDI elevation data. Forest height (h_V) as well as extinction (σ) were then derived from the RVoG model using φ and correlation coefficient ($|\tilde{\gamma}|$) as inputs. Moderate agreement was found between the heights derived using cloud-free GEDI vs. lidar canopy heights, with r^2 of 0.39 (leaf-on) / 0.32 (leaf-off), 0.53 and 0.38 respectively at HBEF, TEF and LSBS (see Fig. 7 and Table 3). Biases were reduced to 2.0 m (leaf-on) / 2.4 m (leaf-off) for HBEF, 1.7 m for TEF and 4.2 m for LSBS. Relatively lower agreement was found when using GEDI under 50% cloud cover, with r^2 of 0.17 (leaf-on) / 0.12 (leaf-off), 0.42 and 0.32, and biases of 2.6 m (leaf-on) / 2.4 m (leaf-off) for HBEF, 2.4 m for TEF and 3.8 m for LSBS. As mentioned earlier, σ represents the attenuation rate of the microwave signal inside the forest volume and reflects the variation of forest scatterer density and dielectric constant. Therefore, compared to case A which used a fixed σ, case B provided improved height estimates by exploiting a spatially varying σ, providing a better fit to the environmental condition at the time of acquisition.

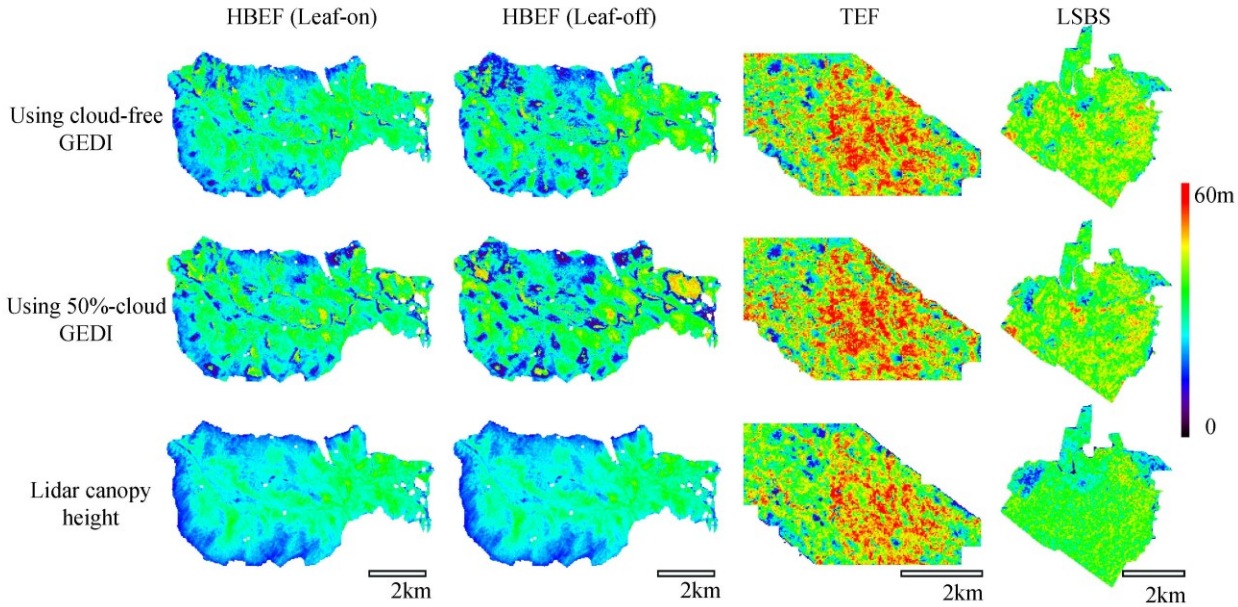

(a)

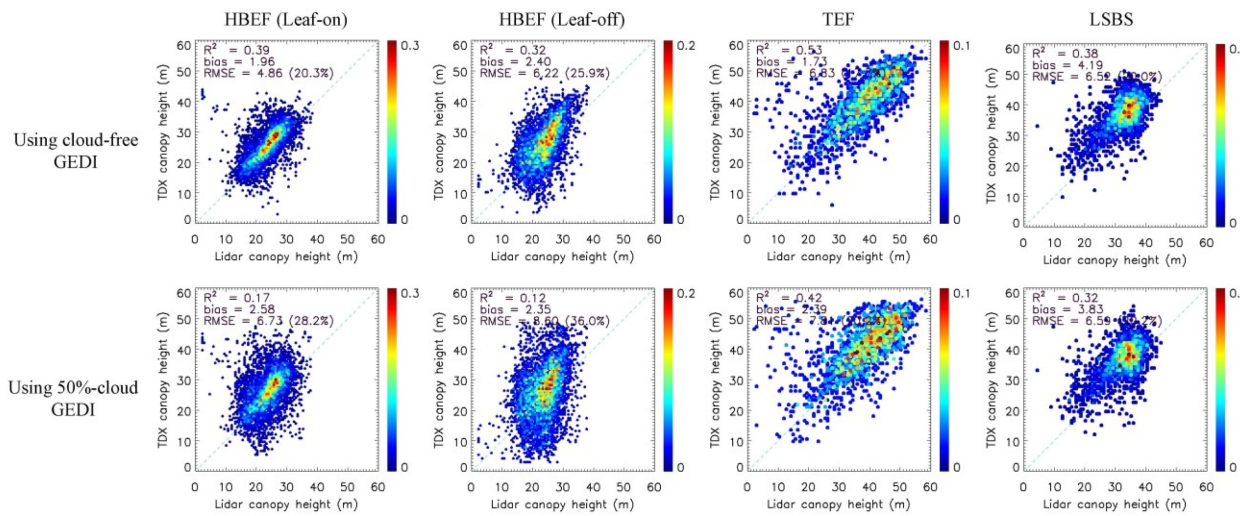

(b)

Fig. 7 (Case B) (a) Forest heights derived from complex TDX coherence using simulated GEDI DTM, based on cloud-free and 50%-cloud cover conditions. (b) Comparisons of the derived heights and reference lidar heights at 90 m resolution.

Table 3. Validation results of RVoG heights from all cases at 90 m resolution.

Cases	Validation Parameters	HBEF				TEF		LSBS	
		Leaf-on		Leaf-off		-		-	
		Cloud-free	50%-cloud	Cloud-free	50%-cloud	Cloud-free	50%-cloud	Cloud-free	50%-cloud
Case A	r^2	0.61		0.57		0.37		0.22	
	Bias (m)	6.41		11.89		4.24		4.89	
	RMSE (m)	7.87		12.70		8.49		7.88	
	RMSE (%)	32.3		52.0		22.0		23.9	
Case B	r^2	0.39	0.17	0.32	0.12	0.53	0.42	0.38	0.32
	Bias (m)	1.96	2.58	2.40	2.35	1.73	2.39	4.19	3.83
	RMSE (m)	4.86	6.73	6.22	8.60	6.83	7.81	6.52	6.59
	RMSE (%)	20.3	28.2	25.9	36.0	17.7	20.2	20.0	20.2
Case C1	r^2	0.51	0.26	0.50	0.21	0.60	0.49	0.43	0.38
	Bias (m)	0.60	0.90	-0.70	-0.80	-1.01	-0.81	0.84	0.28
	RMSE (m)	3.95	5.56	4.21	6.60	6.03	6.65	4.66	5.03
	RMSE (%)	16.5	23.2	17.5	27.5	15.6	17.1	14.2	15.4
Case C2	r^2	0.70	0.37	0.68	0.31	0.56	0.42	0.44	0.39
	Bias (m)	-0.42	0.12	0.17	0.94	-0.69	-0.51	0.55	0.19
	RMSE (m)	2.63	4.03	2.66	4.98	6.12	7.14	4.30	4.64
	RMSE (%)	10.9	16.7	11.1	20.7	15.9	18.5	13.1	14.2

4.3 Cases C1 and C2 – Using simulated GEDI DTM and canopy heights

As described in 3.2, simulated GEDI observations of DTM and canopy height were combined to assist the parameterization of RVoG based on two approaches, either refining σ alone (case C1) or σ and μ combined (case C2).

For case C1, simulated GEDI-derived extinction coefficient (σ) values were employed. Compared to case B which just used the external GEDI-derived DTM, the constraining of σ from additional GEDI height information enhanced the single-pol inversion as expected. When using cloud-free GEDI observations, improved correlation between estimated height and lidar reference was obtained, with r^2 of 0.51 (leaf-on) / 0.50 (leaf-off), 0.60 and 0.43 respectively at HBEF, TEF and LSBS. Biases were reduced to 0.6 m (leaf-on) / -0.7 m (leaf-off) for HBEF, -1.0 m for TEF and 0.8 m for LSBS. The RMSEs were 4.0 m (relative error of 17% for leaf-on) / 4.2 m (18% for leaf-off), 6.0 m (16%), and 4.7 m (14%) respectively (see Fig. 8, Table 3). When using GEDI under 50% cloud cover, height estimates were also improved compared to case B under the same GEDI coverage, with r^2 of 0.26 (leaf-on) / 0.21 (leaf-off), 0.49 and 0.38 respectively at HBEF, TEF and LSBS. Biases of 0.9 m (leaf-on) / -0.8 m (leaf-off), -0.8 m and 0.3 m, and RMSEs of 5.6 m (relative error of 23% for leaf-on) / 6.6 m (28% for leaf-off), 6.7 m (17%) and 5.0 m (15%) were found for the three sites (see Fig. 8, Table 3). These results showed that by constraining σ estimation alone using local tree height information from GEDI, single-pol RVoG height inversion is significantly improved under a μ=0 assumption.

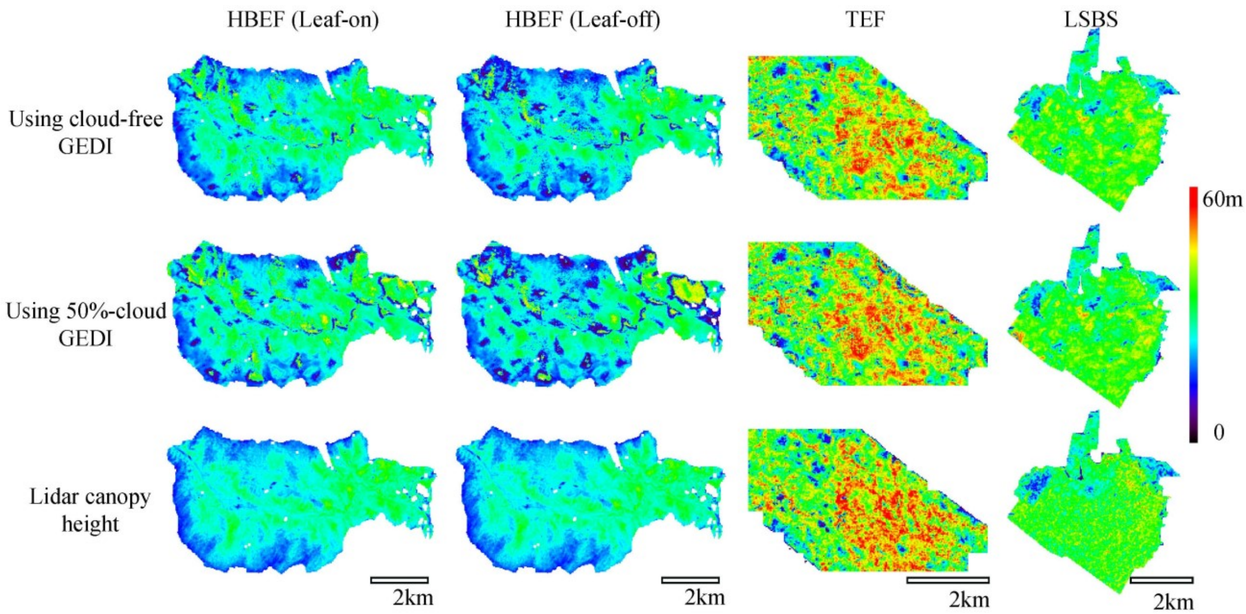

(a)

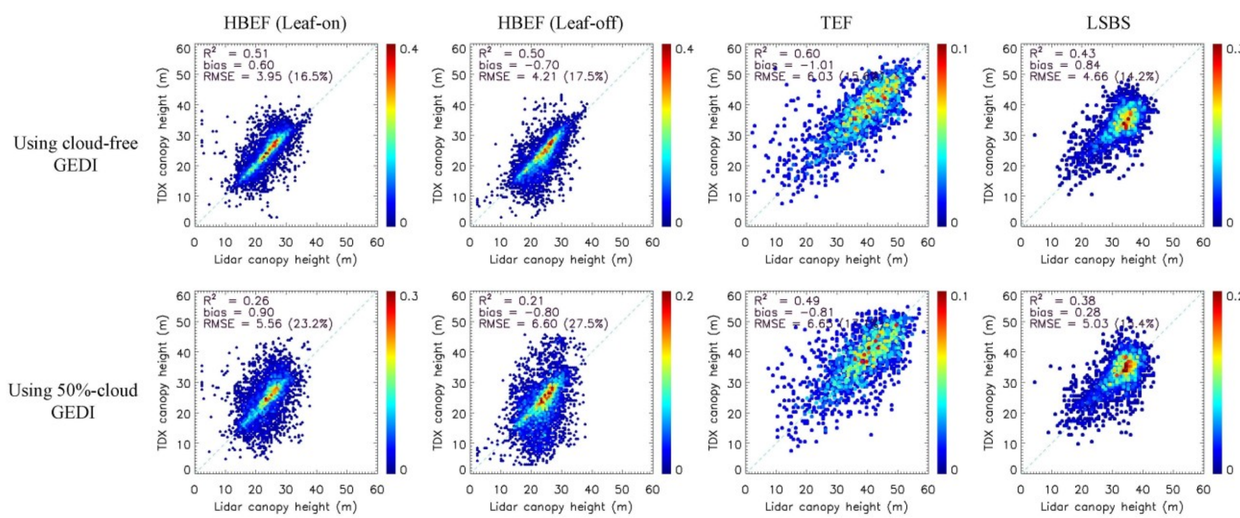

(b)

Fig. 8 (Case C1) (a) Forest heights derived from complex TDX coherence using DTM and canopy height derived from simulated GEDI observations, respectively based on cloud-free and 50%-cloud conditions, to constrain σ. (b) Comparisons of the derived heights and reference lidar heights at 90 m resolution.

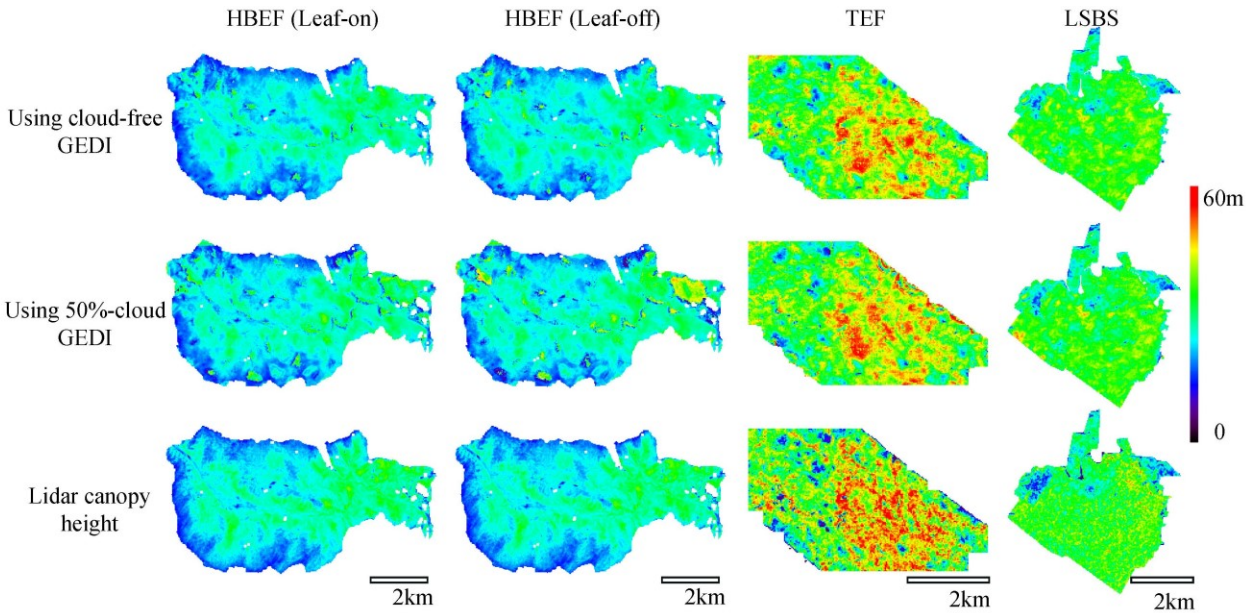

(a)

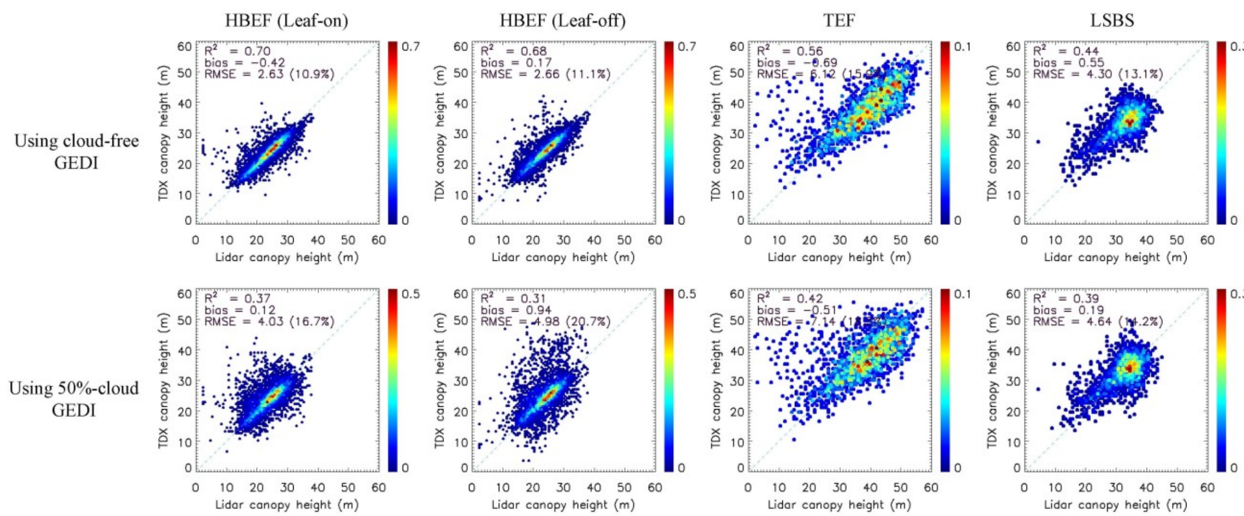

(b)

Fig. 9 (Case C2) (a) Forest heights derived from complex TDX coherence using DTM and canopy height derived from simulated GEDI observations, respectively based on cloud-free and 50%-cloud cover conditions, to constrain σ and μ. (b) Comparisons of the derived heights and reference lidar heights at 90 m resolution.

The second method (case C2) was the only approach that derived both extinction coefficient (σ) and ground-to-volume amplitude ratio (μ) values to improve the height inversion. This was made possible by adding both simulated GEDI canopy height and GEDI-derived DTM as inputs. These σ and μ values were interpolated and used jointly to calculate forest height from the complex coherence ($\tilde{\gamma}$). The estimated heights were improved at HBEF relative to all other cases. When using cloud-free GEDI data, we found r^2 values of 0.70 (leaf-on) / 0.68 (leaf-off), biases of -0.4 m (leaf-on) / 0.2 m (leaf-off) and RMSEs of 2.6 m (11% for leaf-on)/ 2.7 m (11% for leaf-off). When using 50% cloud-cover GEDI data, r^2 of 0.37 (leaf-on) / 0.31 (leaf-off), biases of 0.1 m (leaf-on) / 0.9 m (leaf-off), and RMSEs of 4.0 m (17% for leaf-on)/ 5.0 m (21% for leaf-off) were observed. For each specific case (from A to C2), leaf-on TDX-derived heights had stronger agreement with reference lidar heights than leaf-off TDX-heights. Somewhat paradoxically, greater improvements were observed from case A to case C2 using leaf-off data at HBEF. This is mainly because leaf-off forests have relatively lower volume scattering and higher ground scattering, and are more likely to violate the μ=0 assumption; therefore, the RVoG model using leaf-off data had greater reliance on GEDI inputs (particularly canopy height) for constraining the σ and μ parameters to accurately invert forest heights.

At TEF and LSBS, case C2 derived heights with r^2 values of 0.44–0.56 (cloud-free)/0.39–0.42 (50%-cloud), biases of -0.7 to 0.6 m (cloud-free)/-0.5 to 0.2 m (50%-cloud), and RMSEs of 4.3–6.1 m (13%–16%, cloud-free)/4.6–7.1 m (14%-19%, 50%-cloud). The overall improvements from case C1 to case C2 were not seen (at TEF) or marginal (at LSBS). This suggests a lower utility of constraining the μ values in improving height estimation over areas where taller trees, higher canopy cover or heterogeneous forest structure prevail (Fig. 9 and Fig. 10; Table 3).

5 Discussion

There is the potential to combine the relatively sparse, footprint level estimates of GEDI with wall-to-wall SAR measurements from TDX to provide continuous estimates of canopy height at much finer spatial resolution than what can be obtained by GEDI alone. Indeed, as currently planned, GEDI will grid its height observations to a required resolution of 1000 m. Our work presented here provides a realistic pathway towards the goal of improved height mapping at these finer resolutions.

Our study explored the efficacy of using simulated GEDI observations in improving TDX estimate of canopy heights. The utility of two GEDI-aided RVoG parameters – extinction coefficient (σ) and ground-to-volume amplitude ratio (μ) – for improving forest height estimation was assessed. These two parameters are related to forest height, density, canopy cover, as well as the dielectric constant of scatterers in a forest, and vary across the landscape in different forest environments. In previous studies, these were mainly derived using full-polarimetric InSAR data at longer-wavelength (such as L-band), which are currently unavailable at the global scale (Hajnsek et al. 2009; Kugler et al. 2015; Neumann et al. 2012). Our study demonstrated that these RVoG parameters can be effectively derived from single-pol TDX data by adding simulated GEDI observations of terrain elevation and canopy height as model inputs, and can be applied to improve forest height estimation over a wide range of forest types and terrain conditions.

In general, height estimates improved as more information was used from GEDI to parameterize the RVoG model (Fig. 10 and Table 3). Our results also demonstrated that height estimation using TDX data acquired in leaf-off conditions could be significantly improved through inclusion of GEDI data, opening up the possibility of using a much broader range of TDX acquistions in temperate deciduous forests. We did not, however, evaluate the impact of using leaf-off GEDI data, which is the focus of a future study.

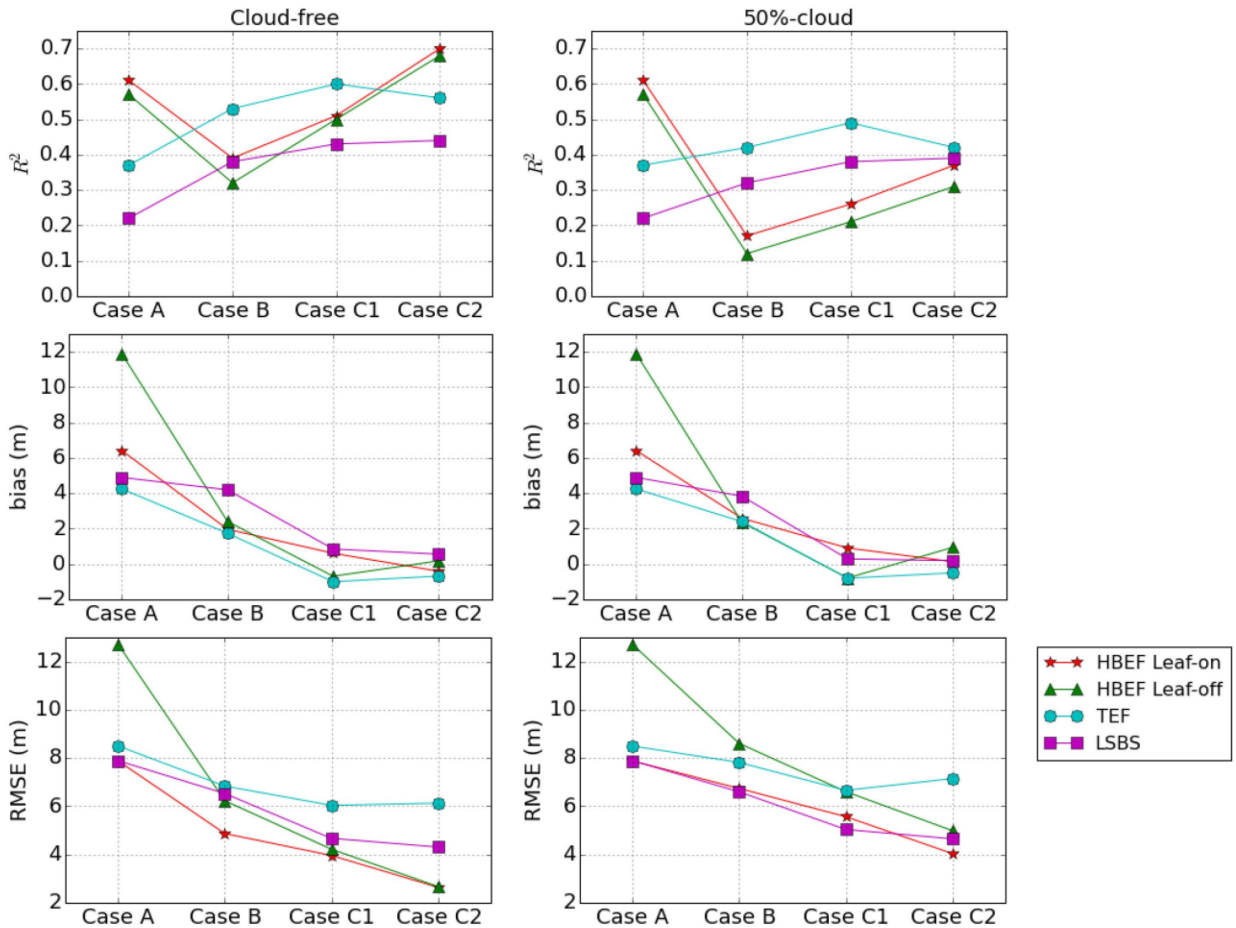

Fig. 10 Different model performance corresponding to the four different cases over HBEF, TEF and LSBS under both cloud-free and 50%-cloud cover conditions.

The fidelity of the GEDI-derived DTM had a significant impact on the efficacy of GEDI/TDX fusion. A key step to providing more accurate height products may be to enhance the GEDI DTM (below canopy topography) (Lee et al. 2018) using, for example, DEM (surface elevation) products from TDX (Bräutigam et al. 2014), SRTM (Rodriguez et al. 2006), Advanced Spaceborne Thermal Emission and Reflection Radiometer (ASTER) (Abrams et al. 2010), or data from future missions such as ICESat-2 (Abdalati et al. 2010) and NASA-ISRO Synthetic Aperture Radar (NISAR) (Hoffman et al. 2016). In particular, the combination of the transect sampling lidar observations from ICESat-2 and GEDI, when combined with continuous, but less accuracte surface elevation meausrements from other missions (Lee et al. 2018), within an improved spatial interpolation/kriging framework is a promising avenue for future research.

Related to this, is the fact that GEDI is limited by cloud-cover and the vagaries of the ISS precessing orbit, which may limit the number of observations available for a given region (and thus lead to an inaccurate DTM, for example, in those areas). When there are insufficient GEDI observations for a given study site, parameters derived over limited GEDI footprints may fail to cover the whole spectrum of forest structure and topographic conditions and may smooth through spatial discontinuities in forest structure (see results in case C2 at TEF and LSBS). GEDI tries to overcome some of this issue by pointing to acquire a more uniform track coverage. Since σ and μ are related to forest structural characteristics, an alternative approach may be to input σ and μ derived from the same TDX acquisition or those with similar geometries (particularly baselines) over similar forest types and environmental conditions that have sufficient lidar coverage. This can be done using segmentation and clustering algorithms to group segments with similar expected σ and μ values, based on TDX coherence and other continuous fields (e.g. canopy cover maps from Landsat) (Clewley et al. 2014). Such fusion approaches are being developed as part of a collaboration between the German Aerospace Center (DLR) and the GEDI mission.

Extrapolation of our results to real data derived from GEDI should be done carefully. Our simulated GEDI data is based on using ALS data, along with the expected ISS track patterns from an earlier 10-beam pattern configuration under cloud-free and 50%-cloud cover conditions within an end-end simulator (Hancock et al. 2019). While the simulator has been validated, the on-orbit data from the GEDI instrument may differ from our simulations.

The change to an eight-beam configuration overall provides about 20% less footprints compared to those from a 10-beam pattern GEDI. However, impact from such change should not be large on our height estimates. In our case C2 particularly, RMSEs increased from the range of 2.6 – 6.2 m (10.9% - 15.9%) to a range of 4.0 – 7.1 m (14.2% - 20.7%) across the three study sites after 50% tracks were removed from the cloud-free track pattern. We would thus expect a smaller impact when 20% tracks (under cloud-free condition) are removed, i.e. results should be better than the cloudy case, where 50% of the tracks are removed, but not as good as assuming we have 10 beams. For example, after using 80% tracks (to simulate the cloud-free condition from eight-beam pattern GEDI) at HBEF, we observed an increased RMSE for Case C2 from 2.6 m (10.9%) to 3.1 m (13.0%).

Note that our simulation regarding beam patterns and clouds in some ways is too conservative. Cloud length scales are such that it's unlikely entire tracks will be eliminated by clouds. Rather, some lidar shots may be obtained through gaps, and so our approach removes more shots than likely happen. That said, the default approach GEDI is implementing is to not use any leaf-off data, and to only use the coverage beams for canopy cover that is less than 70%. In our simulation for HBEF we simply assumed we could use all the leaf-off data, but presented results separately to provide an estimate of how well one could improve height estimates and resolution, via fusion with TDX, if such data are used. Interestingly, because the current configuration now has two strong beams and one coverage vs. one strong and two coverage, more GEDI footprints should be usable under high canopy cover during daytime conditions, which mitigates some of the loss that occurs by going from 10 to 8 tracks.

Another source of potential error is geolocation uncertainty. The geolocation accuracy of GEDI footprints is estimated to be around 7 m at the 1-sigma level. This geolocation uncertainty was not modeled in our experiments. Such error may lead to a less-accurate DTM generation for scattering phase (φ) estimation over sloping surfaces and less-representative RVoG parameters of σ (and μ) over heterogeneous forest structure, and thereby lower the inversion accuracy. Minimizing geolocation uncertainty for GEDI has been a priority during mission development precisely so we may preserve our ability to do fusion at fine spatial scales with other data.

One major application of height estimates (and the main driver behind the GEDI mission) is forest AGB estimation. Previous studies have identified a height accuracy requirement of about 1 m to 2 m at 100 m to 1000 m resolution (with finer resolution more favorable) for effective biomass estimates (Hall et al. 2011; Hurtt et al. 2010; Qi and Dubayah 2016). Our fusion results at 90 m do not quite meet that requirement. However, one of the most important results is that fusion greatly reduces bias. This is key because if bias can be kept low, the fused heights can be aggregated to a coarser resolution until the desired height accuracies are achieved. For example, starting from the 30 m resolution at which the GEDI/TDX fusion was conducted, our height products from case C2 agreed with reference lidar heights (for the purpose of cross validation, heights over simulated GEDI tracks were excluded from comparison; same for the 200 m resolution) at RMSEs of (leaf-on / leaf-off) 3.0 m / 3.3 m at HBEF, 7.8 m at TEF and 5.8 m at LSBS under cloud-free conditions. After averaging up to 200 m, RMSEs were improved to 2.0 m / 2.1 m at HBEF, 3.8 m at TEF and 3.4 m at LSBS under cloud-free conditions. These results demonstrated that keeping biases low enables aggregation to scales that are still relatively fine, and which now approach accuracy requirements. In turn, these observations can then potentially be used to drive models that estimate biomass at scales considerably below 1 km and with accuracies presumably better than what TDX can achieve by itself, as will be explored in subsequent research.

6 Conclusions

We have investigated the fusion of simulated Global Ecosystem Dynamics Investigation (GEDI) lidar data with actual TanDEM-X (TDX) InSAR data to improve forest structure mapping over three contrasting forest types covering a wide range of heights, canopy cover and topography. Our results showed that forest height retrievals from TDX single-polarization InSAR acquisitions based on the widely Random Volume over Ground (RVoG) were significantly improved using GEDI observations of bare-ground topography and canopy top height as inputs to constrain the model parameterization. Improving TDX height estimates with the aid of GEDI measurements is a meaningful step towards deriving blended height products from the two missions with better accuracy and coverage than using either data source alone. These height products, if sufficiently accurate, should improve the potential use of these data for applications such as biomass modeling and biodiversity.

Acknowledgements

This study was funded by NASA's Earth and Space Science Fellowship Program (Grant # 5268930) and NASA's Global Ecosystem Dynamics Investigation mission. We appreciate the Microwaves and Radar Institute of the German Aerospace Center (DLR) for providing the TanDEM-X data and for the assistance in data processing. We are especially grateful to Dr. Kostas Papathanasiou and Dr. Matteo Pardini for their useful comments on this research. We also thank

Dr. Chengquan Huang, Dr. Feng Zhao and Dr. Min Feng for providing the forest disturbance data products.

References

Abdalati, W., Zwally, H.J., Bindschadler, R., Csatho, B., Farrell, S.L., Fricker, H.A., Harding, D., Kwok, R., Lefsky, M., Markus, T., Marshak, A., Neumann, T., Palm, S., Schutz, B., Smith, B., Spinhirne, J., & Webb, C. (2010). The ICESat-2 laser altimetry mission. *Proceedings of the IEEE, 98*, 735-751

Abdullahi, S., Kugler, F., & Pretzsch, H. (2016). Prediction of stem volume in complex temperate forest stands using TanDEM-X SAR data. *Remote Sensing of Environment, 174*, 197-211

Abrams, M., Bailey, B., Tsu, H., & Hato, M. (2010). The aster global dem. *Photogrammetric Engineering and Remote Sensing, 76*, 344-348

Askne, J.I.H., Fransson, J.E.S., Santoro, M., Soja, M.J., & Ulander, L.M.H. (2013). Model-based biomass estimation of a hemi-boreal forest from multitemporal TanDEM-X acquisitions. *Remote Sensing, 5*, 5574-5597

Baccini, A.G.S.J., Goetz, S.J., Walker, W.S., Laporte, N.T., Sun, M., Sulla-Menashe, D., Hackler, J., Beck, P.S.A., Dubayah, R., Friedl, M.A., Samanta, S., & Houghton, R.A. (2012). Estimated carbon dioxide emissions from tropical deforestation improved by carbon-density maps. *Nature Climate Change, 2*, 182-185

Bergen, K.M., Goetz, S.J., Dubayah, R.O., Henebry, G.M., Hunsaker, C.T., Imhoff, M.L., Nelson, R.F., Parker, G.G., & Radeloff, V.C. (2009). Remote sensing of vegetation 3-D structure for biodiversity and habitat: Review and implications for lidar and radar spaceborne missions. *Journal of Geophysical Research: Biogeosciences, 114*, 13

Blackard, J.A., Finco, M.V., Helmer, E.H., Holden, G.R., Hoppus, M.L., Jacobs, D.M., Lister, A.J., Moisen, G.G., Nelson, M.D., Riemann, R., Ruefenacht, B., Salajanu, D., Weyermann, D.L., Winterberger, K.C., Brandeis, T.J., Czaplewski, R.L., McRoberts, R.E., Patterson, P.L., & Tymcio, R.P. (2008). Mapping US forest biomass using nationwide forest inventory data and moderate resolution information. *Remote Sensing of Environment, 112*, 1658-1677

Blair, J.B., & Hofton, M.A. (1999). Modeling laser altimeter return waveforms over complex vegetation using high-resolution elevation data. *Geophysical Research Letters, 26*, 2509-2512

Brolly, M., Simard, M., Tang, H., Dubayah, R.O., & Fisk, J.P. (2016). A Lidar-Radar Framework to Assess the Impact of Vertical Forest Structure on Interferometric Coherence. *IEEE Journal of Selected Topics in Applied Earth Observations and Remote Sensing, 9*, 5830-5841

Bräutigam, B., Bachmann, M., Schulze, D., Tridon, D.B., Rizzoli, P., Martone, M., Gonzalez, C., Zink, M., & Krieger, G. (2014). TanDEM-X global DEM quality status and acquisition completion. In, *Geoscience and Remote Sensing Symposium (IGARSS), 2014 IEEE International* (pp. 3390-3393): IEEE

Caicoya, A.T., Kugler, F., Hajnsek, I., & Papathanassiou, K. (2012). Boreal forest biomass classification with TanDEM-X. In, *Geoscience and Remote Sensing Symposium (IGARSS), 2012 IEEE International* (pp. 3439-3442): IEEE

CEOS (2014). *CEOS Strategy for Carbon Observations from Space. The Committee on Earth Observation Satellites (CEOS) Response to the Group on Earth Observations (GEO) Carbon Strategy.*: JAXA and I&A Corporation

Clark, D.B., & Kellner, J.R. (2012). Tropical forest biomass estimation and the fallacy of misplaced concreteness. *Journal of Vegetation Science, 23*, 1191-1196

Clark, D.B., Olivas, P.C., Oberbauer, S.F., Clark, D.A., & Ryan, M.G. (2008). First direct landscape-scale measurement of tropical rain forest Leaf Area Index, a key driver of global primary productivity. *Ecology Letters, 11*, 163-172

Clark, M.L., Roberts, D.A., Ewel, J.J., & Clark, D.B. (2011). Estimation of tropical rain forest aboveground biomass with small-footprint lidar and hyperspectral sensors. *Remote Sensing of Environment, 115*, 2931-2942

Clewley, D., Bunting, P., Shepherd, J., Gillingham, S., Flood, N., Dymond, J., Lucas, R., Armston, J., & Moghaddam, M. (2014). A Python-Based Open Source System for Geographic Object-Based Image Analysis (GEOBIA) Utilizing Raster Attribute Tables. *Remote Sensing, 6*, 6111-6135

Cloude, S.R., Chen, H., & Goodenough, D.G. (2013). Forest height estimation and validation using Tandem-X polinsar. In, *IEEE International Geoscience and Remote Sensing Symposium (IGARSS)* (pp. 1889-1892)

Cloude, S.R., & Papathanassiou, K.P. (2003). Three-stage inversion process for polarimetric SAR interferometry. *IEE Proceedings-Radar, Sonar and Navigation, 150*, 125-134

Coyle, D.B., Stysley, P.R., Poulios, D., Clarke, G.B., & Kay, R.B. (2015). Laser transmitter development for NASA's Global Ecosystem Dynamics Investigation (GEDI) lidar. In, *Proc. SPIESPIE Optical Engineering+ Applications* (pp. 961208-961208): International Society for Optics and Photonics

Davidson, F.M., & Sun, X.L. (1988). Gaussian approximation versus nearly exact performance analysis of optical communication systems with PPM signaling and APD receivers. *IEEE Transactions on Communications, 36*, 1185-1192

Downs, R., & Day, F. (2005). *National Geographic Almanac of Geography*.

Drake, J.B., Dubayah, R.O., Clark, D.B., Knox, R.G., Blair, J.B., Hofton, M.A., Chazdon, R.L., Weishampel, J.F., & Prince, S.D. (2002). Estimation of tropical forest structural characteristics using large-footprint lidar. *Remote Sensing of Environment, 79*, 305-319

Drake, J.B., Knox, R.G., Dubayah, R.O., Clark, D.B., Condit, R., Blair, J.B., & Hofton, M. (2003). Above-ground biomass estimation in closed canopy Neotropical forests using lidar remote sensing: factors affecting the generality of relationships. *Global Ecology and Biogeography, 12*, 147-159

Dubayah, R.O., Sheldon, S.L., Clark, D.B., Hofton, M.A., Blair, J.B., Hurtt, G.C., & Chazdon, R.L. (2010). Estimation of tropical forest height and biomass dynamics using lidar remote sensing at La Selva, Costa Rica. *Journal of Geophysical Research: Biogeosciences, 115*, 17

Duncanson, L.I., Dubayah, R.O., Cook, B.D., Rosette, J., & Parker, G. (2015a). The importance of spatial detail: Assessing the utility of individual crown information and scaling approaches for lidar-based biomass density estimation. *Remote Sensing of Environment, 168*, 102-112

Duncanson, L.I., Dubayah, R.O., & Enquist, B.J. (2015b). Assessing the general patterns of forest structure: quantifying tree and forest allometric scaling relationships in the United States. *Global Ecology and Biogeography, 24*, 1465-1475

Fatoyinbo, T.E., & Simard, M. (2013). Height and biomass of mangroves in Africa from ICESat/GLAS and SRTM. *International Journal of Remote Sensing, 34*, 668-681

Goetz, S.J., & Dubayah, R.O. (2011). Advances in remote sensing technology and implications for measuring and monitoring forest carbon stocks and change. *Carbon Management, 2*, 231-244

Goovaerts, P. (2000). Geostatistical approaches for incorporating elevation into the spatial interpolation of rainfall. *Journal of hydrology, 228*, 113-129

Hajnsek, I., Kugler, F., Lee, S.K., & Papathanassiou, K.P. (2009). Tropical-forest-parameter estimation by means of Pol-InSAR: The INDREX-II campaign. *IEEE Transactions on Geoscience and Remote Sensing, 47*, 481-493

Hall, F.G., Bergen, K., Blair, J.B., Dubayah, R.O., Houghton, R., Hurtt, G., Kellndorfer, J., Lefsky, M., Ranson, J., Saatchi, S., Shugart, H.H., & Wickland, D. (2011). Characterizing 3D vegetation structure from space: Mission requirements. *Remote Sensing of Environment, 115*, 2753-2775

Hancock, S., Armston, J., Hofton, M., Sun, X., Tang, H., Duncanson, L., Kellner, J., & Dubayah, R. (2019). The GEDI simulator: A large-footprint waveform lidar simulator for calibration and validation of spaceborne missions. *In review for Earth and Space Science*

Hancock, S., Disney, M., Muller, J.P., Lewis, P., & Foster, M. (2011). A threshold insensitive method for locating the forest canopy top with waveform lidar. *Remote Sensing of Environment, 115*, 3286-3297

Hoffman, J.P., Shaffer, S., & Perkovic-Martin, D. (2016). NASA L-SAR instrument for the NISAR (NASA-ISRO) Synthetic Aperture Radar mission. In, *Earth Observing Missions and Sensors: Development, Implementation, and Characterization IV* (p. 988108): International Society for Optics and Photonics

Hofton, M.A., Minster, J.B., & Blair, J.B. (2000). Decomposition of laser altimeter waveforms. *IEEE Transactions on Geoscience and Remote Sensing, 38*, 1989-1996

Hu, T., Su, Y., Xue, B., Liu, J., Zhao, X., Fang, J., & Guo, Q.J.R.S. (2016). Mapping global forest aboveground biomass with spaceborne LiDAR, optical imagery, and forest inventory data*, 8*, 565

Huang, C., Goward, S.N., Masek, J.G., Thomas, N., Zhu, Z., & Vogelmann, J.E. (2010). An automated approach for reconstructing recent forest disturbance history using dense Landsat time series stacks. *Remote Sensing of Environment, 114*, 183-198

Huang, W., Sun, G., Dubayah, R.O., Zhang, Z., & Ni, W. (2012). Mapping forest above-ground biomass and its changes from LVIS waveform data. In, *IEEE International Geoscience and Remote Sensing Symposium (IGARSS)* (pp. 6561-6564)

Hurtt, G.C., Fisk, J., Thomas, R.Q., Dubayah, R.O., Moorcroft, P.R., & Shugart, H.H. (2010). Linking models and data on vegetation structure. *Journal of Geophysical Research: Biogeosciences, 115*, 11

Isenberg, M. (2011). LAStools—Efficient Tools for LiDAR Processing. In. http://www.cs.unc.edu/~isenburg/lastools/

Keller, M., Palace, M., & Hurtt, G. (2001). Biomass estimation in the Tapajos National Forest, Brazil - Examination of sampling and allometric uncertainties. *Forest Ecology and Management, 154*, 371-382

Kellndorfer, J.M., Walker, W.S., LaPoint, E., Bishop, J., Cormier, T., & Fiske, G. (2012). NACP aboveground biomass and carbon baseline data (NBCD 2000), U.S.A. Data set. In: Oak Ridge, Tennessee, U.S.A.: ORNL DAAC

Krieger, G., Moreira, A., Fiedler, H., Hajnsek, I., Werner, M., Younis, M., & Zink, M. (2007). TanDEM-X: A satellite formation for high-resolution SAR interferometry. *IEEE Transactions on Geoscience and Remote Sensing, 45*, 3317-3341

Kugler, F., Lee, S.K., Hajnsek, I., & Papathanassiou, K.P. (2015). Forest height estimation by means of Pol-InSAR data inversion: The role of the vertical wavenumber. *IEEE Transactions on Geoscience and Remote Sensing, 53*, 5294-5311

Kugler, F., Sauer, S., Lee, S.K., Papathanassiou, K., & Hajnsek, I. (2010). Potential of TanDEM-X for forest parameter estimation. In, *European Conference on Synthetic Aperture Radar (EUSAR)* (pp. 1-4): VDE

Kugler, F., Schulze, D., Hajnsek, I., Pretzsch, H., & Papathanassiou, K.P. (2014). TanDEM-X Pol-InSAR performance for forest height estimation. *IEEE Transactions on Geoscience and Remote Sensing, 52*, 6404-6422

Lavalle, M., & Hensley, S. (2015). Extraction of structural and dynamic properties of forests from polarimetric-interferometric SAR data affected by temporal decorrelation. *IEEE Transactions on Geoscience and Remote Sensing, 53*, 4752-4767

Lee, S.K., Fatoyinbo, T., Qi, W., Hancock, S., Armston, J., & Dubayah, R.O. (2018). GEDI and TanDEM-X fusion for 3D forest structure parameter retrieval. In, *International Geoscience and Remote Sensing Symposium*. Valencia, Spain: IEEE GRSS

Lee, S.K., & Fatoyinbo, T.E. (2015). TanDEM-X Pol-InSAR inversion for mangrove canopy height estimation. *IEEE Journal of Selected Topics in Applied Earth Observations and Remote Sensing, 8*, 3608-3618

Lee, S.K., Kugler, F., Papathanassiou, K.P., & Hajnsek, I. (2013). Quantification of temporal decorrelation effects at L-band for polarimetric SAR interferometry applications. *IEEE Journal of Selected Topics in Applied Earth Observations and Remote Sensing, 6*, 1351-1367

Lei, Y., & Siqueira, P. (2015). An Automatic Mosaicking Algorithm for the Generation of a Large-Scale Forest Height Map Using Spaceborne Repeat-Pass InSAR Correlation Magnitude. *Remote Sensing, 7*, 5639

Maselli, F., & Chiesi, M. (2006). Evaluation of statistical methods to estimate forest volume in a Mediterranean region. *IEEE Transactions on Geoscience and Remote Sensing, 44*, 2239-2250

Nelson, R., Margolis, H., Montesano, P., Sun, G., Cook, B., Corp, L., Andersen, H.-E., deJong, B., Pellat, F.P., Fickel, T., Kauffman, J., & Prisley, S. (2017). Lidar-based estimates of aboveground biomass in the continental US and Mexico using ground, airborne, and satellite observations. *Remote Sensing of Environment, 188*, 127-140

Neumann, M., Saatchi, S.S., Ulander, L.M.H., & Fransson, J.E.S. (2012). Assessing performance of L-and P-band polarimetric interferometric SAR data in estimating boreal forest above-ground biomass. *IEEE Transactions on Geoscience and Remote Sensing, 50*, 714-726

NOAA. Daily Record of Climatological Observations. In: National Oceanic and Atmospheric Administration

Olesk, A., Voormansik, K., Vain, A., Noorma, M., & Praks, J. (2015). Seasonal differences in forest height estimation from interferometric TanDEM-X coherence data. *IEEE Journal of Selected Topics in Applied Earth Observations and Remote Sensing, 8*, 5565-5572

Pan, Y., Birdsey, R.A., Fang, J., Houghton, R., Kauppi, P.E., Kurz, W.A., Phillips, O.L., Shvidenko, A., Lewis, S.L., & Canadell, J.G. (2011). A large and persistent carbon sink in the world's forests. *Science, 333*, 988-993

Papathanassiou, K.P., & Cloude, S.R. (2001). Single-baseline polarimetric SAR interferometry. *IEEE Transactions on Geoscience and Remote Sensing, 39*, 2352-2363

Papathanassiou, K.P., & Cloude, S.R. (2003). The effect of temporal decorrelation on the inversion of forest parameters from Pol-InSAR data. In, *IEEE International Geoscience and Remote Sensing Symposium (IGARSS)* (pp. 1429-1431)

Persson, H.J., Olsson, H., Soja, M.J., Ulander, L.M., & Fransson, J.E. (2017). Experiences from large-scale forest mapping of Sweden using TanDEM-X data. *Remote Sensing, 9*, 1253

Pierce, L.E., Walker, W.S., Dobson, M.C., Hunsaker, C.T., Fites-Kaufman, J.A., & Dubayah, R.O. (2002). Fusion of Optical and SAR data for forestry applications in the Sierra Nevada of California. In, *IEEE International Geoscience and Remote Sensing Symposium (IGARSS)* (pp. 1771-1773)

Qi, W., & Dubayah, R.O. (2016). Combining Tandem-X InSAR and simulated GEDI lidar observations for forest structure mapping. *Remote Sensing of Environment, 187*, 253-266

Rodriguez, E., Morris, C.S., & Belz, J.E. (2006). A global assessment of the SRTM performance. *Photogrammetric Engineering & Remote Sensing, 72*, 249-260

Saatchi, S.S., Harris, N.L., Brown, S., Lefsky, M., Mitchard, E.T.A., Salas, W., Zutta, B.R., Buermann, W., Lewis, S.L., Hagen, S., Petrova, S., White, L., Silman, M., & Morel, A. (2011). Benchmark map of forest carbon stocks in tropical regions across three continents. *Proceedings of the National Academy of Sciences, 108*, 9899-9904

Schlund, M., von Poncet, F., Kuntz, S., Schmullius, C., & Hoekman, D.H. (2015). TanDEM-X data for aboveground biomass retrieval in a tropical peat swamp forest. *Remote Sensing of Environment, 158*, 255-266

Schwarz, P.A., Fahey, T.J., Martin, C.W., Siccama, T.G., & Bailey, A. (2001). Structure and composition of three northern hardwood-conifer forests with differing disturbance histories. *Forest Ecology and Management, 144*, 201-212

Siccama, T.G., Fahey, T.J., Johnson, C.E., Sherry, T.W., Denny, E.G., Girdler, E.B., Likens, G.E., & Schwarz, P.A. (2007). Population and biomass dynamics of trees in a northern hardwood forest at Hubbard Brook. *Canadian Journal of Forest Research, 37*, 737-749

Smith, T.F., Rizzo, D.M., & North, M. (2005). Patterns of mortality in an old-growth mixed-conifer forest of the southern Sierra Nevada, California. *Forest Science, 51*, 266-275

Soja, M.J., Persson, H., & Ulander, L.M.H. (2014). Estimation of boreal forest biomass from two-level model inversion of interferometric TanDEM-X data. In, *IEEE International Geoscience and Remote Sensing Symposium (IGARSS)* (pp. 3398-3401)

Soja, M.J., & Ulander, L.M.H. (2013). Digital canopy model estimation from TanDEM-X interferometry using high-resolution lidar DEM. In, *IEEE International Geoscience and Remote Sensing Symposium (IGARSS)* (pp. 165-168)

Solberg, S., Astrup, R., Breidenbach, J., Nilsen, B., & Weydahl, D. (2013). Monitoring spruce volume and biomass with InSAR data from TanDEM-X. *Remote Sensing of Environment, 139*, 60-67

Stysley, P.R., Coyle, D.B., Kay, R.B., Frederickson, R., Poulios, D., Cory, K., & Clarke, G. (2015). Long term performance of the High Output Maximum Efficiency Resonator (HOMER) laser for NASA's Global Ecosystem Dynamics Investigation (GEDI) lidar. *Optics & Laser Technology, 68*, 67-72

Sun, G., Ranson, K.J., Guo, Z., Zhang, Z., Montesano, P., & Kimes, D. (2011). Forest biomass mapping from lidar and radar synergies. *Remote Sensing of Environment, 115*, 2906-2916

Swatantran, A., Dubayah, R.O., Roberts, D., Hofton, M.A., & Blair, J.B. (2011). Mapping biomass and stress in the Sierra Nevada using lidar and hyperspectral data fusion. *Remote Sensing of Environment, 115*, 2917-2930

Tang, H., Brolly, M., Zhao, F., Strahler, A.H., Schaaf, C.L., Ganguly, S., Zhang, G., & Dubayah, R.O. (2014). Deriving and validating Leaf Area Index (LAI) at multiple spatial scales through lidar remote sensing: A case study in Sierra National Forest, CA. *Remote Sensing of Environment, 143*, 131-141

Tang, H., Dubayah, R.O., Swatantran, A., Hofton, M., Sheldon, S., Clark, D.B., & Blair, B. (2012). Retrieval of vertical LAI profiles over tropical rain forests using waveform lidar at La Selva, Costa Rica. *Remote Sensing of Environment, 124*, 242-250

Treuhaft, R.N., Goncalves, F., dos Santos, J.R., Keller, M., Palace, M., Madsen, S.N., Sullivan, F., & Graca, P. (2015). Tropical-forest biomass estimation at X-band from the spaceborne TanDEM-X interferometer. *IEEE Geoscience and Remote Sensing Letters, 12*, 239-243

Van Doorn, N.S., Battles, J.J., Fahey, T.J., Siccama, T.G., & Schwarz, P.A. (2011). Links between biomass and tree demography in a northern hardwood forest: a decade of stability and change in Hubbard Brook Valley, New Hampshire. *Canadian Journal of Forest Research, 41*, 1369-1379

Whitehurst, A.S., Swatantran, A., Blair, J.B., Hofton, M.A., & Dubayah, R.O. (2013). Characterization of canopy layering in forested ecosystems using full waveform lidar. *Remote Sensing, 5*, 2014-2036